

1 **Pressure-Stimulated Rock Current as Loading Diorite to Failure: Particular Variation**
2 **and Holistic Mechanisms**

3 **Wenfei Mao^{1,2}, Lixin Wu^{1,2*}, Youyou Xu^{1,2}, Rubing Yao^{1,2}, Jingchen Lu^{1,2}, Licheng Sun³,**
4 **and Yuan Qi^{1,2}**

5 ¹ School of Geoscience and Info-Physics, Central South University, Changsha, 410083, China.

6 ² Laboratory of Geo-Hazards Perception, Cognition and Predication, Central South University,
7 Changsha, 410083, China.

8 ³ School of Resource and Safety Engineering, Central South University, Changsha, 410083, China.

9 Corresponding author: Lixin Wu (wulx66@csu.edu.cn)

10 **Key Points:**

- 11 • Pressure-stimulated rock current (PSRC) increases in a step-like way at high stress level
12 • PSRC oscillates with maximum amplitudes of several hundreds of nA at the very last
13 instant just before rock failure
14 • Positive hole activation, crack charge separation, and moving charged dislocation
15 contributes comprehensively to the PSRC variations.

16 Abstract

17 The variations in the electric property of loaded rocks are essential in understanding the rock
18 dynamics and fracturing process. Decades of laboratory experiments have revealed different
19 behaviors of stress-stimulated electric current due to the effects of rock types, loading modes, and
20 detection methods. These different behaviors result in difficulties in revealing the underlying
21 physics of electric current in rock and explaining adequately the wide variety of electric precursors
22 measured before rock failure or geohazards. In this study, cubic- and conical-shaped diorite
23 specimens were specially designed and produced to investigate experimentally the characteristics
24 of pressure-stimulated rock current (PSRC) in the process of loading rock specimen to failure. We
25 measured a particular phenomenon of diorite PSRC variation with pressure, that is, PSRC
26 remained nearly stable until the applied stress reached 83%–98% of the failure strength. A
27 remarkable step-like increment in PSRC was uncovered, and drastic oscillations with maximum
28 amplitudes of several hundreds of nA happened one second prior to abrupt rock failure. A holistic
29 mechanism that includes positive hole activation, field emission of electrons due to crack charge
30 separation, and moving charged dislocation was applied to interpret this particular phenomenon.
31 We found that these mechanisms contribute comprehensively rather than individually to the
32 evolution of PSRC. We expect to provide an improved understanding of the underlying physics of
33 PSRC and the variation in rock electric property.

34 Plain Language Summary

35 Many kinds of electric precursors of rock fracturing or rock failure have been experimentally
36 revealed in past four decades. Therein, the behaviors of stress stimulated electric current of rock
37 materials are influenced by the loading modes and current detection methods; thus, different
38 mechanisms were proposed accordingly. By uniaxially and partly compressing cubic- and conical-
39 shaped diorite specimens to failure, we revealed the particular and significant variations of rock
40 current before the rock failure, and found that such behaviors were attributed to a combination of
41 several mechanisms rather than a single one. This study exhibits potential use of dynamic signal
42 detection of pressure stimulated rock current and possible precursor identification of rock
43 fracturing.

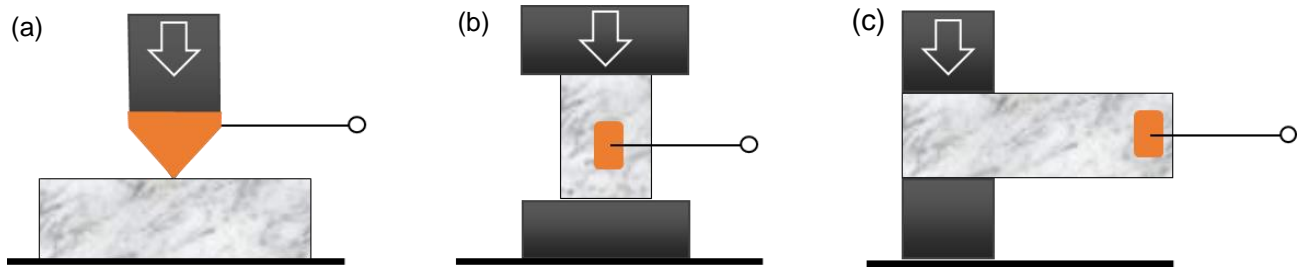
44 1 Introduction

45 Rock dynamic disasters, such as rock bursts and tectonic earthquakes, result originally from deep rock
46 fracturing or rock failure and occur frequently from a deep part of the ground to the surface. Although
47 electric and magnetic phenomena was observed before some volcano and seismic activities (Uyeda et al.,
48 2002), and many geoscientists and rock engineers have attempted to place various sensors in rock mass to
49 search for early warning of the occurrence of rock failure or geohazards (Liao et al., 2003; Meng et al.,
50 2015), it is difficult or ineffective due to the uncertainty of the detected signals and the complexity of the
51 underground environment. Many laboratorial experiments have been performed to investigate the potential
52 electric precursors of rock failure, and they have revealed several electric signals, including charge particles
53 (Enomoto and Hashimoto, 1990, 1992), surface potential (Hadjicontis and Mavromatou, 1994; Yoshida et
54 al., 1997, 1998; Freund, 2002; Li et al., 2020), and electric currents (Hoenig, 1979; Vallianatos et al, 1999;
55 Stavrakas et al., 2004; Triantis et al., 2006, 2012; Freund et al., 2006; Anastasiadis et al., 2007; Li et al.,
56 2015; Li et al., 2021a, 2021b), preceding or accompanying with rock failure. The generation of electric
57 current in stressed rock (called in brief as rock current) is believed to be associated with the micro-fracturing
58 inside the rock volume, and mechanisms including electrokinetic effects (Mizutani et al., 1976),
59 piezoelectricity (Warwich et al., 1982), field emission of electrons (Enomoto and Hashimoto, 1990, 1992),
60 moving charged dislocation (Slifkin, 1993; Hadjicontis and Mavromatou, 1994; Vallianatos and Tzanis,

61 1998) and peroxy defects activation (Freund, 2002, 2006) have been proposed. In many experiments, such
62 electric signals are measured when the stress applied to the rock sample exceeds the yield stress (Yoshida
63 et al., 1997; Yoshida et al., 1998; Starrakas et al., 2004; Anastasiadis et al., 2007; Li et al., 2015; Pasiou
64 and Triantis, 2017), but other experiments have shown that electric signals are generated immediately upon
65 the application of any significant mechanical load (Freund et al., 2006; Scoville et al., 2015; Li et al., 2021a,
66 2021b). Thus, proper interpretation and physical understanding of the differences in electric signals are
67 very necessary.

68 A review of experimental studies in the past three decades, indicates that two major factors are
69 responsible for the differences mentioned above. First, different rock types have different mechanical
70 properties due to the complex mineral compositions and structures of rocks. Thus, even under the same
71 stress condition, rock specimens present different features of electric signals. For instance, in a tri-axial
72 deformation experiment performed by Yoshida et al. (1998), the electric potential on a dry sandstone
73 surface changed markedly prior to dynamic rupture, but such a change was not observed in dry basalt. The
74 researchers concluded that the piezoelectric effect is the dominant sources of precursory electric signals.
75 Many other experiments have demonstrated that a marble sample emits observable pressure-stimulated rock
76 currents (PSRC) when the progressive uniaxial stress exceeds its linear elasticity limit, and PSRC increases
77 considerably and reaches the maximum value in the vicinity of rock failure (Stavrakas et al., 2004).
78 However, similar experiments on sandstone have demonstrated that weak currents are generated
79 instantaneously when a load is applied initially, and PSRC corresponds well to the stress variations (Li et
80 al., 2021b).

81 Second, applying different loading and detection modes also influences the detected electric signals in
82 experiments. Figure 1 illustrates three classic loading modes that were commonly applied in the past three
83 decades. In the early 1990s, Enomoto and Hashimoto (1990; 1992) measured the emission of charged
84 particles from rocks undergoing indentation fracturing (Fig. 1a). Given that the indenter served as an
85 electrode, the collected charged particles were highly associated with indentation fracturing; thus, intensive
86 electric signals were concentrated where strong acoustic signals appeared. The amounts of detected
87 electrons and negative ions were higher than that of positive ions when rock cracking occurred around the
88 indenter. Figure 1b shows the most widely used loading mode in rock mechanics experiments, in which the
89 entire rock specimen is loaded. Aside from the effects caused by rock types, many other factors, including
90 loading rate (Hadjiconitis and Mavromatou, 1994; Li et al., 2020), moisture of rock specimens (Yoshida et
91 al., 1998; Saltas et al., 2018), Young modulus of rock specimens (Stavrakas et al., 2004; Triantis et al.,
92 2006; Li et al., 2020), strain rate (Triantis et al., 2012), and deformation stage (Li et al., 2021b), have been
93 experimentally confirmed to exert remarkable impacts on PSRC or electric potentials. However, the
94 position of electrodes pasted or mounted on a specimen may also affect experimental results. For instance,
95 when the electrodes are pasted on the side surface of a sandstone specimen (Li et al., 2021b), PSRC initially
96 increases rapidly then decreases slowly a few seconds later; afterward, PSRC increases very slowly until it
97 approaches final failure and reaches the maximum when rupture occurs. Meanwhile, when the electrodes
98 are pasted on the press head of the loading machine (Li et al., 2020), the PSRC variation is divided into
99 three stages, namely, including rapid growth, slow growth, and approaching the peak. As shown in Fig. 1c,
100 the partly loading and detection mode was first adopted by Enomoto and Hashimoto in 1992 by considering
101 the ignorable distance between the initial rock fracturing (usually in deep Earth) and ground surface or the
102 stress gradients from concentration zone to relaxation zone; this mode has been developed and widely used
103 since 2002 (Freund, 2002, 2006, 2009; Scoville et al., 2015; Li et al., 2021a). When only one end or a sub-
104 volume of a rock specimen is subjected to external loads, detectable electric currents or potentials can be
105 measured on the other end or in the stress-free section. Usually, the electric signals are generated
106 immediately upon the application of any significant mechanical load. However, under the influence of the
107 stress concentration effect, macroscopic fracture of a specimen in the third mode (Fig. 1c) occurs initially
108 along the press head edge, and the stress of the rock volume is much less than the rock failure strength.
109 Thus, previous experiments have mainly focused on the elastic deformation phase of rocks, and the
110 evolution of electric signals with sufficient fracturing of rock sub-volume has rarely been investigated and
111 remains unclear.



112 **Figure 1. Schematic of three classic loading modes applied in experiments to detect electric charges generated**
 113 **from rock specimens.** The orange legends represent the commonly applied position of electrodes. (a) Indentation
 114 loading at one point. (b) Loading over the entire cross section. (c) Loading partly on one end or a sub-volume.
 115

116 The variation in electric signals detected from loaded rock specimens is a reflection of the
 117 generation and redistribution of charge carriers inside rock volumes or on rock surfaces. The
 118 inhomogeneous mechanical property of rock specimens and the position of electrodes placed
 119 influence the features of detected electric signals. The acoustic emission (AE) detection technique
 120 is often used to investigate the relationship between micro-fracturing events and electric signals
 121 because the electrification by micro-fracturing is generally considered as the predominate
 122 mechanism (Stergiopoulos et al., 2013; Pasiou and Triantis, 2017; Saltas et al., 2018). However,
 123 during the loading of a rock specimen, the received AE signals reflect all of the micro-fracturing
 124 events occurring inside the entire rock volume, whereas the electrodes pasted on the sample surface
 125 generally receive the electric signals induced by nearby opening fractures. The relation between
 126 AE and electric signals entails much uncertainty and needs to be investigated further.

127 This study focused on the third loading mode (Fig. 1c) and aim to clarify the PSRC precursors
 128 of rocks partly compressed to fracturing. First, a special-shaped rock specimen was prepared to
 129 reduce or eliminate the stress concentration effect, and ensure that the loaded sub-volume could
 130 be broken sufficiently. Second, progressive compression was applied until rock failure occurred.
 131 During the progressive compression, the PSRC from the entire loaded sub-volume to the unloaded
 132 upper part and the AE signals were recorded simultaneously. Lastly, the holistic mechanisms of
 133 diorite PSRC were examined.

134 2 Materials and Methods

135 2.1 Specimen preparation

136 Gray diorite, from Fujian Province, China, was used to create the rock specimens. The thin section
 137 of the diorite indicates that the diorite is composed of 60% plagioclase, 10% potassium feldspar,
 138 10% pyroxene, and 10% –15% biotite and amphibole (Fig. S1a). In contrast to granite that was
 139 commonly adopted in previous experiments, diorite was used in our experiment for three reasons.
 140 First, the sizes of the mineral grains in diorite are relatively uniform, and the mechanical property
 141 under external loading is homogeneous. Second, few quartz grains are contained in diorite, so the
 142 piezoelectric effect on the electric signals can be excluded to reduce the uncertainty in data
 143 analysis. Lastly, the proxy defect is common in diorite, which is also a typical igneous rock like
 144 granite. Thus, PSRC can be measured due to P-hole activation by compressive stress even if no
 145 other mechanism is involved. To reduce or eliminate the stress concentration effect along the press
 146 head edge and ensure that the loaded rock sub-volume could be fractured sufficiently, we created
 147 a bar-shaped rock specimen with a conical head, as shown in Fig. S1b. The lower part is for
 148 uniaxial and compressive loading, and the upper conical part is unloaded and provides a small top
 149 plane. For uniaxial compressive loading, the “unparallelism” of two loading surfaces was less than

150 0.05mm. In addition, the surface of specimen was polished with 400-mesh sandpaper. To prevent
151 water from affecting the rock specimen, we placed them in an oven whose temperature increased
152 to 120 °C for several days until the specimen's weight remained unchanged.

153 As shown in Fig. S1c, five strain gauges were pasted on one of the prepared diorite specimens
154 to investigate the basic mechanical property of the specimen. The results are illustrated in Fig. S1d.
155 The deformations in the different regions exhibited considerable differences. The deformation of
156 the loaded volume was significant, but no considerable strain occurred at the upper unloaded end,
157 suggesting that the specimen was loaded partly and the upper part was approximately unstressed.
158 In the process of loading to failure, the deformations of the side surface were nearly linear, and
159 unstable deformations occurred several seconds before specimen failure. This result indicates that
160 the diorite specimens were typical brittle materials. At the subsequent loading stage, the axial
161 direction of the underside was severely compressed, and lateral deformation was released suddenly
162 due to the unstable cracking, indicating the significant lateral expansion of the specimen. The
163 specimen was broken suddenly and completely when the stress reached the peak stress (136 MPa),
164 illustrating that the stress concentration effect along the press head edge was eliminated with such
165 a loading mode.

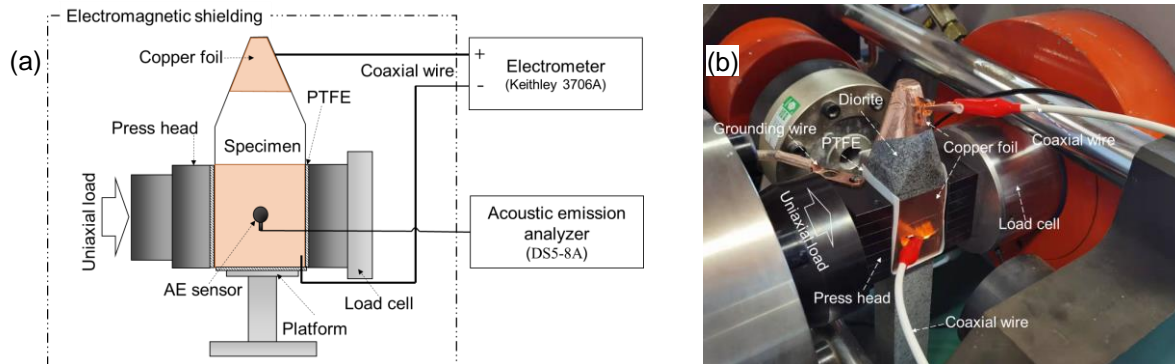
166 2.2 Experiment setup

167 The experiment setup is shown schematically in Fig. 2. A rock specimen was placed on a
168 platform, and its lower edge was at the same height as the press head. Conductive copper foil with
169 a thickness of 0.06mm was pasted tightly on the rock surface to receive electric charges. The
170 specimen was electrically isolated from the press heads and platform by thin
171 polytetrafluoroethylene (PTFE) pads (thickness of 0.6 mm), which can also absorb machine noise.
172 An AE sensor was bonded to the flat specimen surfaces. Before mounting the AE sensor, a
173 transparent tape was placed on the copper foil so that the charges generated in the loaded specimen
174 and collected by the copper foil would not be influenced by the metal AE sensor. Meanwhile, a
175 suitable amount of Vaseline was applied between the probe and the transparent tape to enhance
176 the reception of AE signals. Considering that electrical signals in the environment exert a
177 substantial impact on the effective measurement of the electric currents of a loaded rock, which
178 was often performed with slight and subtle variations in previous studies, we conducted the
179 experiments in a closed electromagnetic shielding cage formed by red copper wire (800 meshes).
180 Two press heads were grounded to release possible charges from the loading machine.

181 A servo-controlled loading machine was used to provide uniaxial compressive stress on the rock
182 specimens. The loading machine was specially designed to deliver a maximal 500 kN axial load
183 with precision higher than $\pm 1\%$. Electric current measurements were carried out with a Keithley
184 3706A electrometer equipped with a multichannel scanner card (Keithley 3721ST). The
185 measurement range was $1\text{pA} - 100\mu\text{A}$ with an accuracy of 1nA . The sampling frequency of the
186 electric signals was 33 Hz. The negative electrode of the electrometer was connected to the copper
187 foil pasted on the lower part of a rock specimen through a coaxial cable (RG 58U), and the positive
188 electrode was connected to the copper foil pasted on the upper part of the specimen. AE signals
189 were detected using DS5-8A system through piezoelectric sensors (RS-2A sensors, 50 – 400 kHz).
190 Pre-amplification of 40 dB was used and the sampling frequency of the AE signals was 3 MSPS.
191 The threshold for the detection of an acoustic event was set to 10 mV.

192 The dried diorite specimens were subjected to progressive loading at a constant rate of 1 kN/s,
193 and the time series of the electric currents and AE signals were recorded simultaneously. The
194 experiments were conducted several times to ensure the reproducibility of the results and the

195 validity of the derived correlations between electrical currents and external loads. After
 196 experiments, the fragments of broken rock specimen used for SEM (TESCAN mira4) were first
 197 cleaned with pure water and paint thinner, with which the greasy dirt and fine particles on the rock
 198 surface were wiped off. Then the samples were dried at 120°C for two hours. All the specimens
 199 were coated with gold (200 thickness) prior to SEM observation in order to prevent surface
 200 charging under the SEM electron beam.



201
 202 **Figure 2. Experiment setup in this study.** (a) Schematic of the experiment setup used for the measurement of
 203 PSRC and acoustic emission during uniaxial loading of diorite specimens. (b) Photograph of a specimen inside
 204 the load frame.

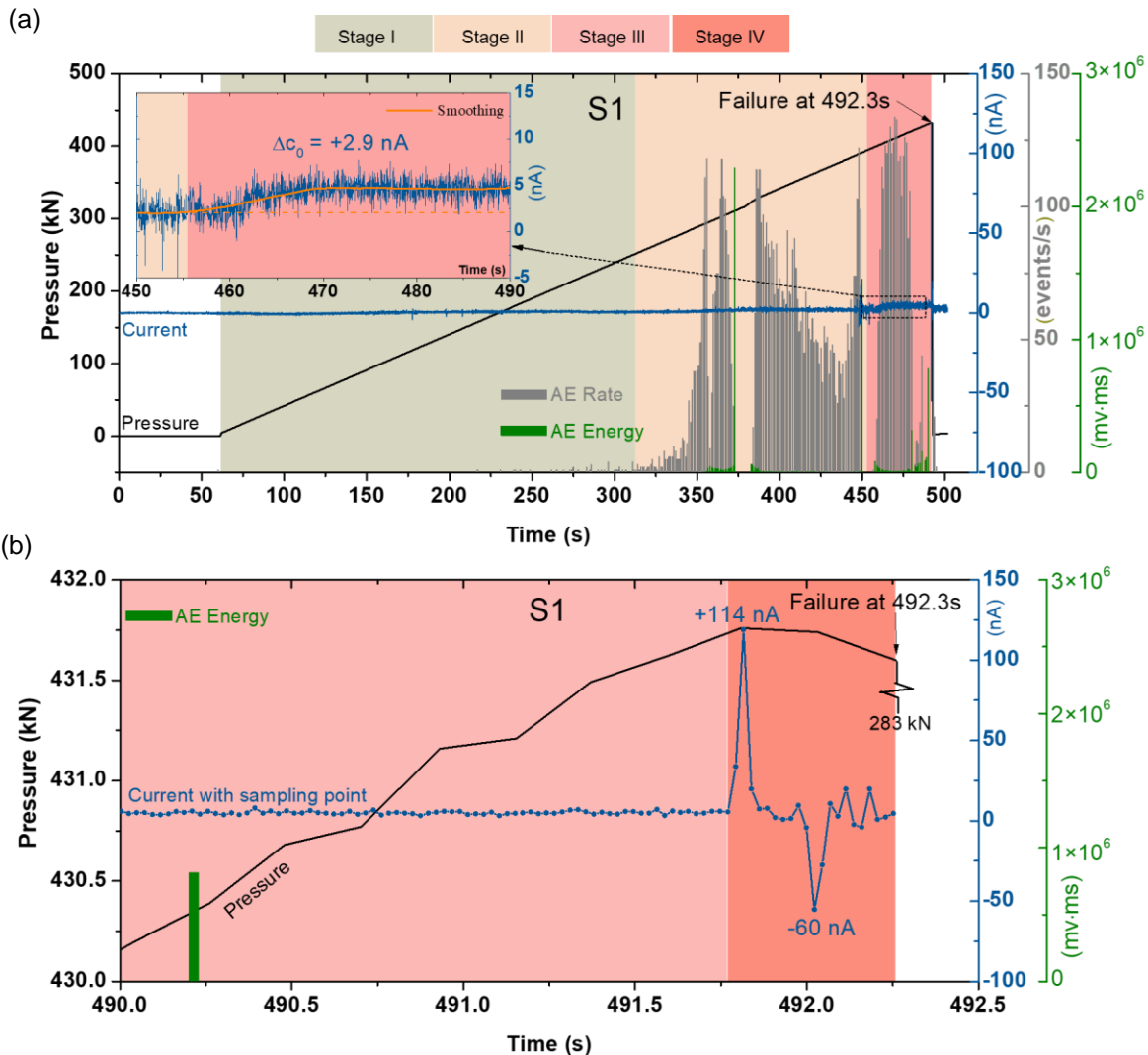
205 3 Results

206 3.1 Experimental setup and procedures

207 The detailed temporal variation of the PSRC flowed through specimen S1 is shown in Fig. 3a.
 208 Before the loading, PSRC was maintained at around 0 nA and showed slight fluctuations, which
 209 were caused and determined by the background noise. The load began to increase at 60 s, but no
 210 remarkable PSRC change appeared. When the load reached 396 kN at 456 s (stress level of 117.6
 211 MPa) and equaled ~91.6% of the failure strength ($\sigma_f = 128$ MPa), a step-like increase in PSRC
 212 was measured, i.e., PSRC increased gradually from 456 s to 469 s then became steady. To express
 213 this step-like increase in PSRC clearly, the originally measured PSRC signals are smoothed and
 214 illustrated by an orange solid line in Fig. 3a. PSRC increased by 2.9 nA (ΔC_0) in the step-like
 215 increment process, after which PSRC remained at high-level values with background noise until it
 216 approached rock failure. As shown in Fig. 3b, PCS began to change dramatically and showed a
 217 sharply positive fluctuation with a huge amplitude of +114 nA at 0.48s before specimen failure.
 218 Afterward, PSRC showed a large negative fluctuation with an amplitude of -60 nA and several
 219 other fluctuations with relatively large amplitudes prior to specimen failure; this result
 220 demonstrates that the PSRC variations prior to rock failure might be determined by the
 221 complicated physical process.

222 The AE signals of S1, which were produced by the rapid growth of microcracks inside the rock
 223 volume, were detected simultaneously (Fig. 3a). In the beginning of loading ($t = 60$ s), only one
 224 AE event occurred, and it was caused by the closure of pre-existing micropores or specimen flaws.
 225 No AE occurred until 217 s, suggesting that the specimen was deformed elastically during this
 226 period. From 217 s to 310 s, microcracks began to develop, and a few scattered AE events
 227 occurred. Physically, these microcracks were isolated and discrete. Continuous, considerable AE
 228 occurred after 310 s, suggesting that the stress-induced microcracking became intense and the

229 microcracks started to nucleate from pre-existing flaws. After 310 s the evolution of AE could be
 230 divided into three relatively separate phases with respect to the AE rate and AE energy. Each phase
 231 began with an intense AE rate and ended with a relatively high AE energy, indicating that an
 232 independent and significant fracturing process occurred inside the specimen. The silence stage
 233 between intensive AE events suggests that the rock specimen was stressed locking. Two seconds
 234 before specimen failure (Fig. 3b), AE was not measured anymore, which indicates that the
 235 specimen was in a state without microcracking but contained huge restored deformation energy
 236 for impending failure.



237
 238 **Figure 3. Detected signals in diorite specimen S1.** (a) Signals measured during the entire loading process and
 239 (b) signals measured several seconds prior to specimen failure, the blue dots represent the sampling points of
 240 electric current.

241 Considering the relationship between the PSRC variations and evolutions of AE events in S1,
 242 we summarize the following points. First, the step-like increase in PSRC was measured at a stress
 243 level of $0.92\sigma_f$, whereas considerable AE activity was measured when the stress ratio was equal
 244 to $0.68\sigma_f$, which is much earlier than the remarkable variation in PSRC and indicates that the step-
 245 like rise in PSRC may be related to the accumulative AE events. Second, although a huge
 246 amplitude of +114 nA and subsequent significant fluctuations were illustrated prior to rock failure,

247 no AE signals were detected during this short period, indicating that the noteworthy PSRC
248 variations prior to rock failure were independent of rock fracturing.

249 On the basis of the features of PSRC and AE measured in the experiments, the entire loading
250 process could be divided into four characteristic stages: early silence stage (stage I), during which
251 the PSRC and AE variations were not considerable; AE developing stage (stage II), during which
252 AE was considerable and even intensive but no remarkable PSRC variations were shown; PSRC
253 rising stage (stage III), during which a step-like rise in PSRC was exhibited and the accumulative
254 AE events and AE energy exceeded 50% of their eventual values; and the final stage (stage IV),
255 which occurred about 1 second prior to abrupt failure and where PSRC showed drastic fluctuations
256 but AE was relatively unchanged.

257 Diorite specimen S1 was broken explosively, several macroscopic fractures were produced
258 parallel to the loading direction, and finely ground rock particles were formed (Fig. 4a and 4b).
259 The lower part of the specimen was laterally dilated by several tensile fractures under compression.
260 Meanwhile, the measured macroscopic tension fractures and the separate fragments indicate that
261 the loaded lower part of the specimen was broken sufficiently. The upper conical end of the
262 specimen was not broken and remained complete, but it was separated explosively from the loaded
263 part by 0.5–1 meter when the specimen reached failure, indicating that the energy released for rock
264 fracturing was considerable. The formation of large fragments of the broken specimen was mainly
265 determined by the axial–parallel fractures, and the destruction of rocks was always accompanied
266 with the formation of separate particles (Viktorov and Kochanov, 2016), which was mainly caused
267 by the linkage of trans-granular cracks to form detached slivers of the broken materials (Fronseak
268 et al., 1985). To investigate the distributions of microcracks in broken S1, SEM observations were
269 performed. The results are illustrated in Figs. 4c–4e. The micrograph of the surface of the upper
270 part (Fig. 4c) indicates that no observable microcracks were distributed; it also suggests that the
271 upper part of the specimen was not influenced by the applied pressure, and the original structures
272 was approximately not changed. By contrast, on the pressed surface (Fig. 4d), a typical tensional
273 microcrack with a width of 2–3 μm that passed across grains was measured. It displayed a
274 characteristic Z-like shape [30], demonstrating that large amounts of microcracks were distributed
275 on the pressed surface in addition to the observable macroscopic fractures. Moreover, the
276 microcracks generated on the freshly fractured surface were interrelated but not sheared (Fig. 4e),
277 and the cracks and crystal cleavages were observable, indicating that the grain-boundary and trans-
278 granular microcracks developed well inside the loaded sub-volume of the specimen.

279 To ensure the reliability of the experimental results, the same tests were performed on six other
280 diorite specimens (S2–S7). The obtained PSRC and AE signals during the loading processes and
281 during several seconds prior to specimen failures are shown in Figs. S2 and S3, respectively. Under
282 the progressive–compressive loading to failure, the evolutions of the PSRC of these specimens
283 could also be divided into three phases similar manner to that of S1. Specifically, PSRC showed a
284 relative plateau in the early loading stage, followed by a typical step-like increment when the stress
285 level reached $0.85\text{--}0.98\sigma_f$. Then, dramatic fluctuations with huge amplitudes occurred in the final
286 stages of the loading process. Accordingly, the entire loading processes of these specimens could
287 be also divided into four stages in a similar way to S1 with respect to the features of PSRC and
288 AE. Notably, the AE activity of each diorite specimen differed. On the one hand, in the diorite
289 specimens prepared for testing, the microscopic cracks, including grain boundary, intergranular
290 and intragranular cracks (Simmons and Richter, 1976), were often irregular and ragged; thus,
291 during the loading process, the microcracking induced by stress concentration (Gallagher et al.,
292 1974; Krzna, 1979), elastic mismatching, (Wang and Heard, 1985) and twinning (Olsson and Peng,

1976) at the microscale was specific. Consequently, the time-dependent behavior of AE activity
 directly related to the evolution of microcracks (Atkinson, 1987) may show differences in AE rate
 and AE energy. On the other hand, the natural geological environment and the sampling processes
 of specimens differ, leading to a difference in their stress history and Kaiser effect (Kurita and
 Fujii, 1979).

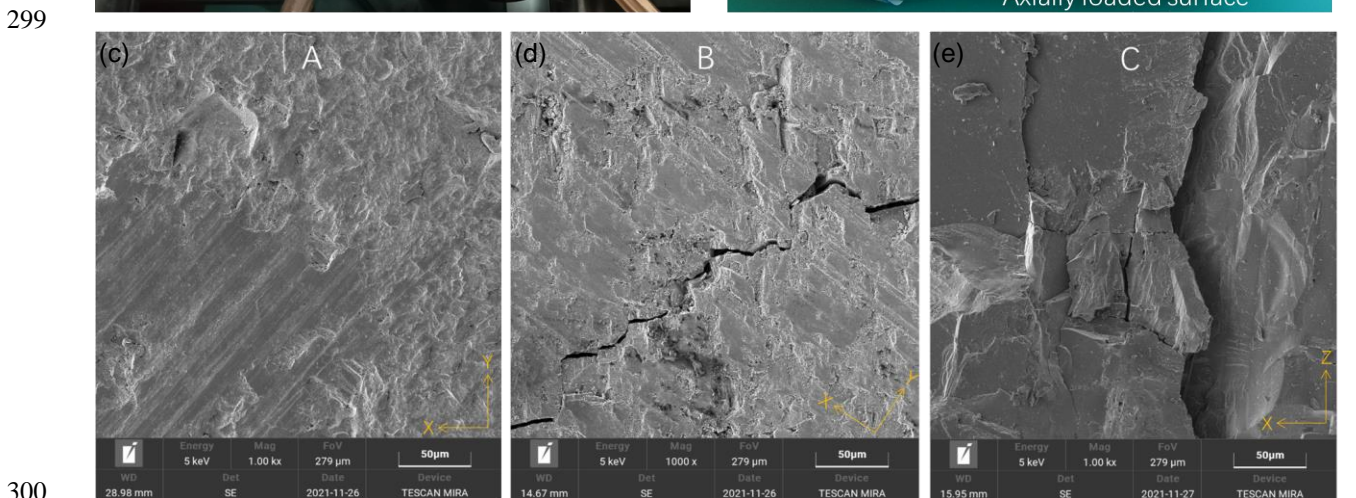
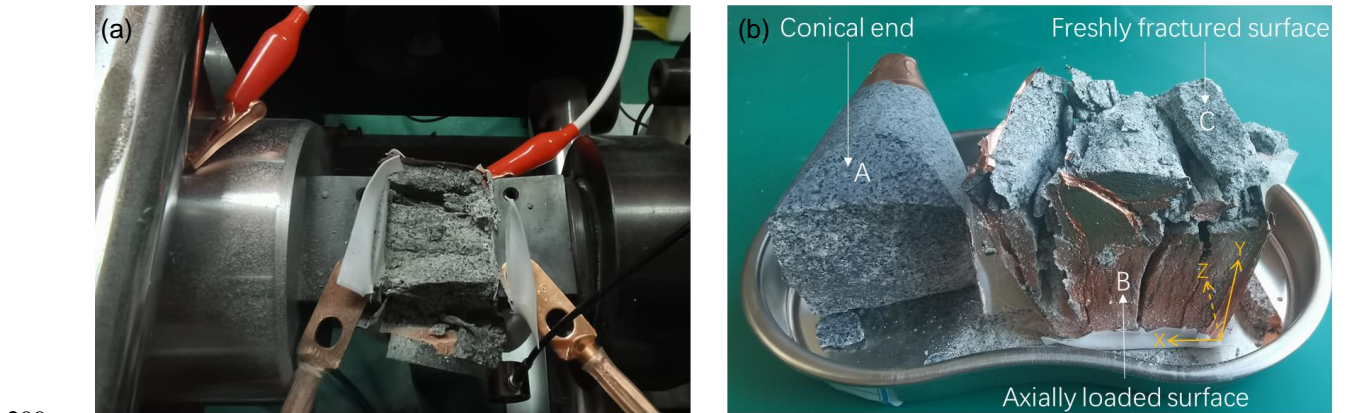
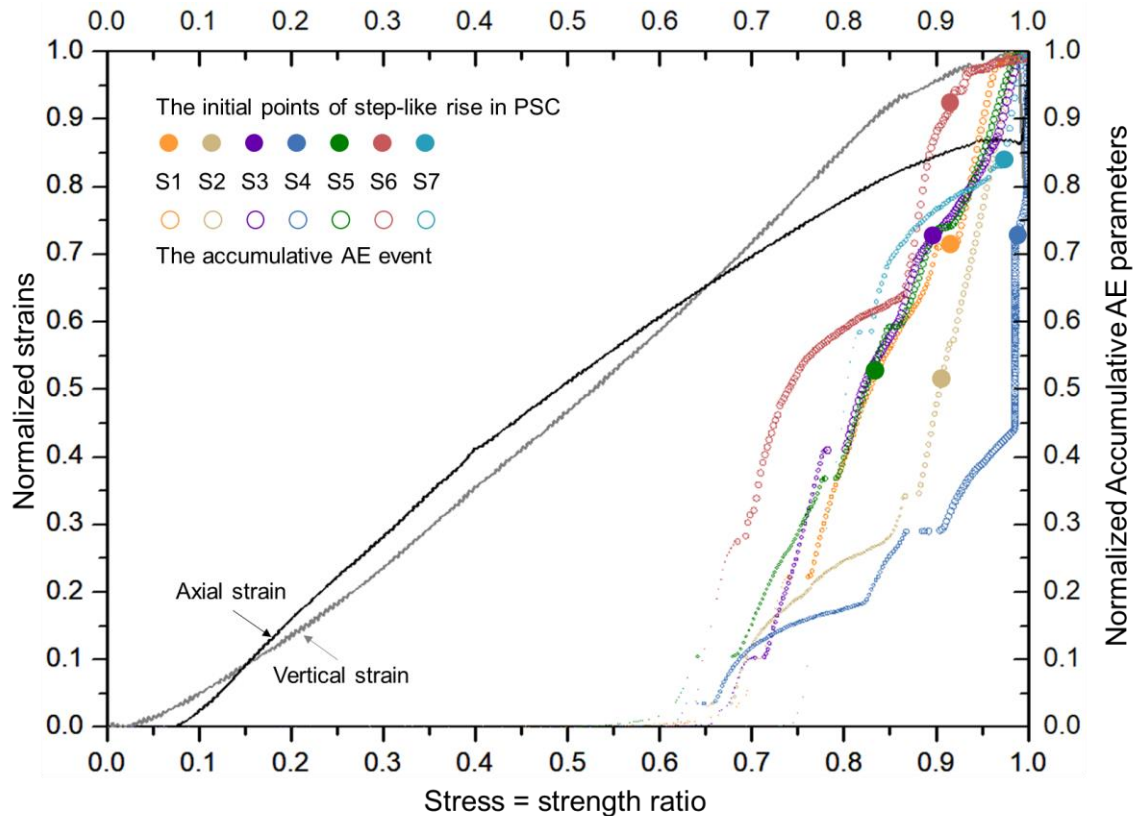


Figure 4. Photos of the broken diorite specimen S1. (a) The conical head separated explosively from the specimen as specimen failure and (b) front surfaces axially loaded in the experiment. (c)-(e) SEM micrographs of different regions on broken specimen S1. “A” illustrates the polished specimen surface at the upper part, “B” illustrates the specimen surface subjected directly to the pressure, and “C” illustrates the freshly fractured surface.

Considering the differences in the behaviors of the AE signals of the specimens, the evolutions of the AE of each specimen were normalized with respect to the total number of events and total energy (Fig. S4). The AE events of all specimens began to increase considerably when the stress level exceeded $0.65\sigma_f$, suggesting that at the early loading stage, the growth of microcracks in all specimens was slight and limited. With the further increase in applied stress, the accumulative AE events of the specimens showed different behaviors. S1, S3, and S5 presented a relatively linear tendency; S2 and S4 showed a gradual increase followed by a rapid increase, and S6 and S7 exhibited a fast–slow–fast increasing trend. Moreover, the evolutions of the accumulative AE energy of the specimens were similar despite the corresponding stress levels. Generally, three sudden increments were exhibited during the entire loading process. Considering the relationships between the step-like rise in PSRC and the applied stresses, the AE behaviors, and the strain changes (shown in Fig. 5), we derived the following conclusions. First, although the initiation of

317 the step-like rise in PSRC corresponds to different stress levels ($\sim 0.84\text{--}0.99\sigma_f$) for different
 318 specimens, the high stress level of loaded specimens is likely to cause a remarkable increase in
 319 PSRC. Second, if the total damage of a given specimen is certain as loading it to failure, then the
 320 accumulation of damage corresponding to at least 50% of the total number of AE events and AE
 321 energy is important for inducing significant PSRC. Third, a specimen is strengthened at the stress
 322 level of $0.85\text{--}0.99\sigma_f$, during which the increase in stress is faster than that in strain; this might be
 323 related to the step-like rise in PSRC. Lastly, the drastic variations in PSRC prior to specimen failure
 324 might be influenced by the abnormal variations of strains at the final loading stage, where the
 325 vertical strain is released suddenly and the axial strain is increased drastically.



326 **Figure 5. Relationships of the step-like rise of PSRC and the applied stress, the strains, the accumulative**
 327 **AE events and the accumulative AE energy.** The sizes of colored circles illustrate the normalized accumulative
 328 AE energy, which behave its maximum at the moment of abrupt final failure.
 329

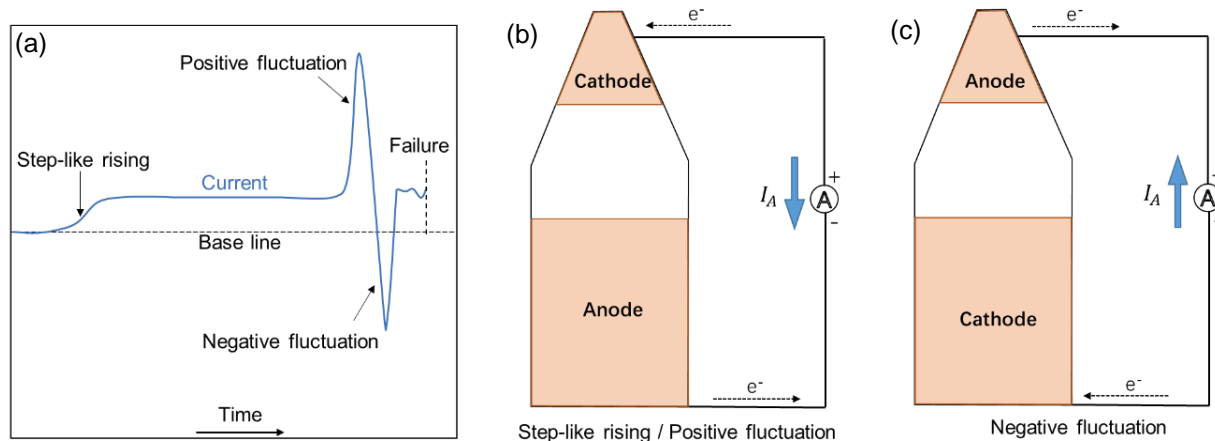
330 Notably, the drastic fluctuations of PSRC in all specimens occurred at the very last instant just
 331 before the maximum failure stress was reached, which is generally within 1 second, and the first
 332 fluctuations were always positive (Fig. S3). This result indicates that the initiation of dramatic
 333 PSRC variations prior to rock failure might have the same physical process for different specimens,
 334 although the failure strength, PSRC variations, and development of micro-fracturing in these
 335 specimens are considerably different. Statistically, the amplitudes of the step-like rise in PSRC for
 336 all specimens in this study were 3–4 nA, and the drastic fluctuations of PSRC that occurred 1
 337 second prior to specimen failure showed wide range of variations with respect to their amplitudes
 338 and directions. Table S1 summarizes the experimental results on the PSRC variations of all
 339 specimens.

340 **4 Discussion**

341 4.1 Battery effect related to PSRC variations

342 By applying uniaxially compressive load on the bar-shaped diorite specimen with a conical head,
 343 the diorite PSRC illustrated obvious features, as shown in Fig. 6a, including (1) step-like rise in
 344 PSRC as the accumulative damage developed to a certain degree; (2) positive fluctuation of PSRC
 345 prior to specimen failure and (3) negative fluctuation for several specimens. Before discussing the
 346 mechanism of these special PSRC variations, we need to know first what physical process these
 347 PSRC variations represent.

348 Generally, the variation in PSRC detected from a loaded rock specimen is a reflection of the
 349 generation and redistribution of charge carries inside rock volumes or on the rock surface. In our
 350 experiments, the negative electrode of the electrometer was connected to the copper foil pasted on
 351 the lower part of the rock specimen, and the positive electrode was connected to the copper foil
 352 pasted on the upper part of the rock specimen. Therefore, in terms of the step-like rise or positive
 353 fluctuation of PSRC, the rock specimen behaved like a battery, as shown in Fig. 6b. The upper
 354 part of the specimen served as the cathode with electrons flowing into it, and the lower part (loaded
 355 end) functioned as the anode with electrons flowing out of it. Similarly, the negative fluctuation
 356 of PSRC demonstrated that the upper part of the specimen behaved as the anode, and the lower
 357 part (loaded end) behaved as the cathode, as shown in Fig. 6c. To investigate the mechanism of
 358 the measured PSRC variations in our experiments, we determined how the applied pressure
 359 induced the differences in potential between the upper and lower parts of the diorite specimen.



360 **Figure 6. Schematic of the battery effect with respect to the PSRC variations measured in the experiments.**
 361 (a) The typical features of PSRC revealed in our experiments. (b) The forward current indicates the upper part
 362 as cathode and lower part as anode, while (c) the reverse current indicates the exchange of specimen's electrodes.
 363

364 4.2 Holistic mechanisms of PSRC from the rock specimen

365 Several mechanisms have been proposed to interpret the electrical signals produced by stressed
 366 rocks and minerals; these mechanisms include field emission of electrons due to crack charge
 367 separation (Enomoto and Hashimoto, 1990), piezoelectric effects (Yoshida et al., 1994),
 368 electrokinetic effects (Mizutani et al., 1976), moving charged dislocations (MCD; Slifkin, 1993;
 369 Hadjicontis and Mavromatou, 1994; Vallianatos and Tzanis, 1998), and outflow of positive holes
 370 (P-hole; Freund, 2002, 2006). The piezoelectric effect refers to the capability of the quartz mineral
 371 to generate an electric charge when rapid stress changes occur due to dynamic rupture. Given that
 372 the tested thin section of diorite (Fig. S2) illustrated that the amount of quartz minerals embodied

373 in the tested diorite was small, we confirmed that the piezoelectric effect was not the cause, at least
374 not the main cause, of the PSRC production in our tests. Electrokinetic phenomena are caused by
375 the presence of an electric double layer formed at the solid–liquid interface, which means the
376 electrokinetic effect needs the participation of liquid. However, the tested specimens in this study
377 were air-dried several days before testing, and diorite usually has low porosity; thus, the
378 electrokinetic effect can be ignored.

379 Field emission of electrons is associated with crack charge separation during rock fracturing.
380 With the opening of a fracture in rock volume, the charges are separated on both sides of the crack,
381 where high electric fields in the order of 10^6 – 10^7 V/cm are produced between the crack walls and
382 result in the field emission of electrons (Enomoto and Hashimoto, 1990, 1992). A perfect
383 correlation between the appearance of electric signals and the occurrence of cracking was
384 measured and confirmed in the indentation loading experiments, and signals related to negatively
385 charged particles (representing electrons or negative ions) and positively charged particles
386 appeared during loading (Enomoto and Hashimoto, 1990, 1992). With the micro- and macro-
387 fracturing of the rock specimen, the effects of crack charge separation or field emission could
388 affect the generation and distribution of electric charges of the rock volume. However, with regard
389 to the crack charge separation mechanism only, our experimental results revealed two
390 controversial phenomena. First, the initiation of considerable AE events did not induce observable
391 variations in PSRC, and AE activity did not show regular variations before and after the step-like
392 rise in PSRC. Second, physically, if the fracture initiated inside the rock volume but did not
393 penetrate onto the rock surface, how did crack charge separation influence the detected PSRC in
394 our experiment? Third, the dramatic PSRC variations that occurred prior to rock failure showed
395 poor relationships with AE activity.

396 The MCD mechanism always occurs in association with brittle fracturing (Vallianatos et al.,
397 2004). In a crystalline structure, charged edge dislocation, which is electrically neutral in thermal
398 equilibrium (Whitworth, 1975), is moved under a dynamic process and no longer maintains
399 neutrality, thereby inducing an electric signal (Slifkin, 1993). An experimental study conducted in
400 1994 reported that a variation in electric signals occurs when the applied stress increases at an
401 increasing rate, but no change in electric signal occurs when the stress increases at a constant rate
402 (Hadjicontis and Mavromatou, 1994). Thereafter, Vallianatos et al. (2004) developed MCD theory
403 and correlated the variation in electric currents to the changing Young's modulus. They found that
404 PSRC only appears when the stress is high enough for the material to enter the plastic deformation
405 phase. The MCD model is generally accepted and has been verified by many experiments on rocks
406 and minerals (Stavrakas et al. 2004; Triantis et al. 2006; Anastasiadis et al. 2007; Stergiopoulos et
407 al. 2015). MCD theory appears to be responsible for the step-like rise in PSRC measured in our
408 experiments. However, providing a reasonable explanation for the potential difference between
409 the upper and lower parts (Fig. 6) is difficult.

410 From a chemical point of view, peroxy defects, which are typically formed with a molecular
411 structure of $O_3X-OO-YO_3$ ($X, Y=Si^{4+}, Al^{3+}$ etc.), are ubiquitous in rock forming minerals of the
412 Earth's crust (Rossman, 1996) and embodied massively in silicates (Freund et al., 2006) and
413 igneous rocks (Freund, 2002; Balk, et al., 2009). The peroxy bond (-OO-) in rock materials can be
414 disturbed by additional stress; as a result, positive holes are produced and propagate from the
415 stressed rock volume to the unstressed parts (Freund et al., 2006; Scoville et al., 2015). Given that
416 diorite is a typical igneous rock and the particular loading and detecting mode applies (Fig. 2), the
417 effect of peroxy defects could be an underlying mechanism of the diorite PSRC measured in our
418 experiments. Scoville et al. (2015) found that upon loading a rock with a constant rate, the current

419 begins to rise rapidly and reaches its maximum at 5 MPa, which is far smaller than rock strength.
 420 However, such a phenomenon did not occur repeatedly in our experiments.

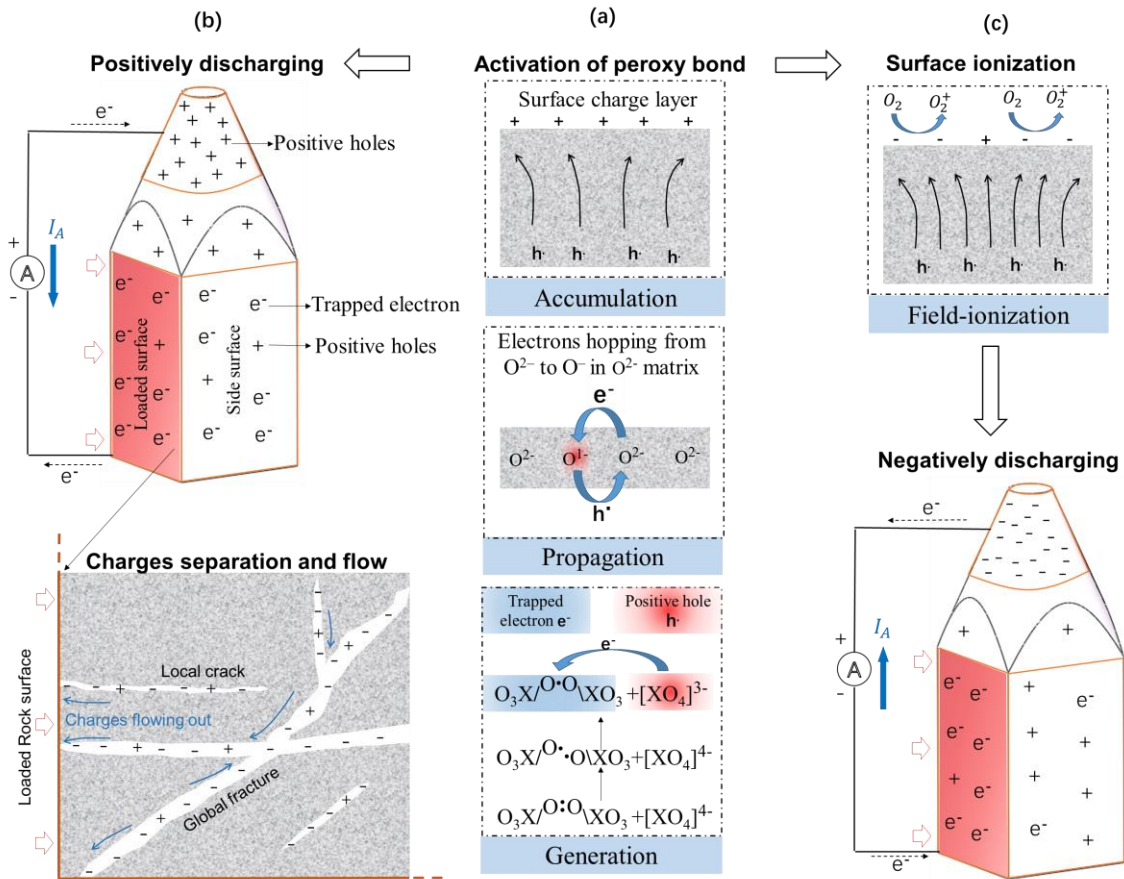
421 Physically, the experimentally detected variations in PSRC could be attributed to a combination
 422 of several mechanisms rather than a single one, and all the possible mechanisms or physical
 423 processes should be considered simultaneously. In the following parts, the contributions of
 424 different mechanisms at different stages are analyzed and discussed in detail.

425 4.3 Step-like rise in PSRC

426 4.3.1 Causes of PSRC remains indistinctive at the first two stages

427 Despite the effects of the loading and detection method applied in our experiments, the theories of
 428 MCD and field emission of electrons can reasonably explain why PSRC kept “silent” at stage I
 429 because no or only a few dislocations or microcracks occurred during this period. However, several
 430 studies have demonstrated that PSRC rises immediately as the specimen is loaded because the
 431 dormant -OO- embodied can be activated when the peroxy bond angle is changed (Freund et al.,
 432 2006; Scoville et al., 2015; Li et al., 2021a, 2021b). In our experiments, a remarkable rise in PSRC
 433 did not occur at the early loading stage. The mineral components of the diorite specimen, namely,
 434 plagioclase, pyroxene and biotite (Fig. S1a), are typical tectosilicate, inosilicate, phyllosilicate
 435 minerals, respectively, within which the structural units of $O_3Si-OO-SiO_3$ bearing dormant peroxy
 436 links (-OO-) are richly embodied (Freund, 2002). Therefore, as shown in Fig. 7a, the low-level
 437 pressure can also disturb the peroxy links and activate h^\bullet , which propagates through the stationary
 438 O^{2-} sublattice; their mutual electrostatic repulsion forces them to the unstressed or less-stressed
 439 surfaces. In fact, the numerical simulation results show that stress is also distributed on the upper
 440 part of specimen (Fig. S6), but the values of stress on upper part are much less than that on lower
 441 part; thus, the stress gradients along with the height of specimen was formed and the h^\bullet propagated
 442 to upper part of specimen. In such case, the upper unloaded volume of the specimen most likely
 443 behaves as the cathode due to the accumulation of h^\bullet . Accompanied with the activation of h^\bullet , the
 444 decoupling peroxy bond receives an electron (e^-) from the neighbouring $[SiO_4]^{4-}$. Freund (2006)
 445 supposed that the trapped e^- is loosely bonded and can move within the stressed rock volume. Thus,
 446 the lower pressed volume behaves as the anode. Once the connection between the upper and lower
 447 parts is established, the circuit loop closes, allowing the electrons to flow out (Fig. 7b).

448 For a given rock type, the amount of stress-activated h^\bullet mainly depends on the stressed volume
 449 of the rock specimen. In laboratory experiments (Freund et al., 2006) on a long granite slab, when
 450 one end (the stressing volume was about 1500 cm^3) of the slab rock was compressed at a constant
 451 rate of 0.1 MPa/s until 67 MPa, the measured PSRC increased linearly at a rate of $10.4 \times 10^{-3}\text{ nA/s}$.
 452 In our experiments, the compressed diorite volume was 161.3 cm^3 , and the loading rate was (0.3
 453 MPa/s. The PSRC induced by h^\bullet is expected to be approximately $1.1 \times 10^{-3}\text{ nA/s}$ about. The impact
 454 of such a small amount of h^\bullet on PSRC was limited and most likely obscured by the background
 455 noise. Consequently, remarkable PSRC variations were difficult to observe at the early loading
 456 stage. Meanwhile, part of stress-activated h^\bullet could also propagate to the less-stressed side and
 457 bottom surfaces. Thus, the amount of net negative charges that could be received by the lower
 458 copper foil was smaller than the amount of h^\bullet flowing into the upper copper foil. The induced
 459 PSRC variation was limited because the electric current flowing through the closed circuit was
 460 physically determined by the relatively small amounts of net negative charges flowing out from
 461 the lower part.



462
 463 **Figure 7. Stress-activated positive hole charge carriers in the partly loaded diorite specimen.** (a) Generation
 464 and propagation of positive hole charge carriers, (b) positively discharging effect, and the local cracks and global
 465 fractures in the lower part of specimen, (c) negatively discharging effect induced by surface ionization.

466 With the increase in compressive stress, the AE activities began to occur when the stress
 467 exceeded $0.6\sigma_f$. At stage II, the microcracks initiated from local stress concentrations resulting
 468 from mismatches in elastic properties along the grain boundaries (Tapponnier and Brace, 1976) or
 469 from natural flaws and pores (Sprunt and Brace, 1974); thus, these microcracks were distributed
 470 discretely as local cracks (Fig. 7b, Fig. S7). As shown in Fig. S8, in the process of fracturing the
 471 peroxy bond embedded in the crack tip would be bent and decoupled, then separated thoroughly.
 472 It is no doubt that h^{\bullet} would be released in the process of bending, and an extra electron would be
 473 trapped at the parent peroxy entities at the same time. With the complete separation of the bond,
 474 the previously trapped electron would occupy the valence band of oxygen as an eight-electron
 475 configuration and become immobile. At the same time, the other unpaired electron behaves as
 476 dangling bond, that are expected to trap the free electrons on or near the freshly created crack wall
 477 surface, i.e., the negative charges separated on the crack walls may be consumed by such dangling
 478 bond (Dickinson et al., 1981). Only when local cracks are generated on or in the vicinity of a
 479 specimen surface, the micro-fracturing induced charges, including crack separation charges and
 480 electrons driven by field emission (Enomoto and Hashimoto, 1990, 1992), could be transferred to
 481 the copper foil, and the total net electrons flowing out the lower part may increase accordingly.
 482 However, our numerical simulation results show that most of the newly generated microcracks at
 483 early loading stage (before $0.85\sigma_f$) were inside the rock volume rather than on the rock surface
 484 (Fig. S7), and notably these local cracks are discrete and isolated; thus, their negative charges

485 could not be transferred to the rock specimen surface at stage II. Therefore, with the comprehensive
486 effects of the reduction in loosely trapped electrons at the parent peroxy entities and the slight
487 increase in negative charges from the rock surface cracks, the PSRC variation was still indistinctive.

488 The above-mentioned MCD mechanism is also associated with micro-fracturing. According to
489 MCD theory, the transient electric variation of a crystalline structure in a dynamic process is
490 related to the non-stationary accumulation of deformations (Vallianatos et al., 2004). When the
491 stress exceeds the elastic limit and micro-cracks begin to generate, actually the rock is still nearly
492 linear if the micro-fracturing activity is very low (Scholz, 1968); thus, PSRC is still not changed.
493 In addition, as illustrated in previous experiments (Stavarakas et al., 2004; Pasiou and Triantis,
494 2017; Li et al., 2021b), the measured currents start to increase after a certain critical stress
495 threshold, but the maximal variations of currents could reach 0.1–0.4 nA, which is much less than
496 the background noise of PSRC in our experiment. Meanwhile, if a crack open inside the stressed
497 rock volume, its impact on the electric signals on the rock surface is limited because the intensity
498 of the electric field decays with distance. Therefore, although the field emission of electrons is
499 truly existed at stage-II in the current study, its effects on PSRC were minimal and limited.

500 4.3.2 Coalescence and connection of microcracks induce remarkable PSRC variations

501 The step-like rise of PSRC in all the specimens started at the stress level of $0.84\text{--}0.99\sigma_f$ and
502 significant cumulative damages were reached (Fig. 5). Hence, we analyzed the characters of stage
503 III with respect to the microstructures and charge distributions of the specimens. Physically, as the
504 compressive loading increased further, many new microcracks are activated, and the existing
505 microcracks continued growing until the size and numbers of the cracks were so large that they
506 began to interfere and interact with each other, eventually linking the surface and inner cracks and
507 forming global fractures (Fig. 7b), which are characteristic of rock specimens approaching failure
508 [35]. We could not investigate the source locations of the microcracks by using one AE sensor
509 only, but the numerical simulation indicates that the evolution of microcracks inside the specimen
510 underwent coalescing and connecting processes at this stage (Fig. S7).

511 In fact, as illustrated in Fig. 7b, in the process of loading diorite specimen several local cracks
512 initiated on the rock surface, during which the electric charges resulting from broken peroxy bonds
513 or charge separations could transfer and flow into the copper foil on the surface. Meanwhile, other
514 local cracks initiated in the inner part of the rock volume; in this case, the free electric charges
515 formed with crack growth were constrained on or near the crack surface or crack tips until these
516 local cracks extended to the specimen surface. In addition, the generation of global fractures at
517 stage III attached to the specimen surface provided channels for the free charges from other local
518 cracks inside the rock volume. On the other hand, at stage III the positive holes were also activated
519 by the cracking behavior and propagated continuously into the upper part. Therefore, with the
520 coalescence and connection of the microcracks, abundant cracking-induced negative charges were
521 transferred to the rock surface and led to the significant increment in PSRC.

522 These discussions suggest that in process of loading the diorite specimen to failure, P-hole
523 activation, crack charge separation, and field emission were facilitated by the coalescence and
524 connection of microcracks at a high level of stress. Notably, the critical stress level and

525 accumulative damage may be influenced strongly by rock types, loading modes, specimen size,
526 and the rock volume subjected to compressive load. These factors will be studied in another work.

527 4.4 Drastic PSRC oscillation prior to rock failure

528 All of the seven diorite specimens showed that drastic PSRC variations occurred one second about
529 prior to rock failure. The physical processes prior to rock failure, especially within such a short
530 period, are difficult to be illustrated clearly because of the impending sudden failure of diorite
531 specimens, and the corresponding fracture mechanics or stress state in the rock volume are also
532 poorly understood. As discussed in Section 4.3, at stage III, the intensive local cracks should have
533 interfered and interacted with each other and developed into multiple groups of global fractures
534 (Atkinson, 1987), which could be distributed throughout the entire rock volume. Thus, assuming
535 that the generation of positive holes at stage III is only related to the opening of local cracks, the
536 amounts of electrons or negative ions at the lower part that result from the broken peroxy bond,
537 charge separations, field emission effect, and MCD effect are much larger than the amounts of
538 positive charges transmitting into the upper part, which results only from the activation of positive
539 holes. Hence, the detected PSRC in this study was determined by the amounts of positive holes at
540 stage III that were kept relatively stable because the generation and consuming rates of positive
541 holes may have a dynamic equilibrium state. As stage IV approached, a few AE signals were
542 detected, and the significant deformation of the specimen was mainly caused by the dislocations
543 or deformations of the lattice inside the mineral grains rather than the growth of microcracks along
544 the grain boundary. Thus, the main generation mechanism of positive holes was changed, and the
545 peroxy bonds embedded inside the mineral grains, the amount of which was much larger than that
546 of the peroxy bonds embedded in the grain boundaries or flaws, might have been activated. PSRC
547 increased drastically when the large amounts of positive holes propagated into the upper part.

548 At stage IV, because almost no local cracks or global fractures occurred accompanying the
549 drastic PSRC variations, the electrons or negative ions reserved in the lower part at stage III were
550 consumed rapidly by the large amounts of upward positive holes. Thus, the detected PSRC
551 returned to zero instantaneously, and a positive fluctuation occurred. Most of the time, large
552 amounts of positive holes accumulated in the upper part. The accumulation of positive hole charge
553 carriers h^\bullet on the surface produced a positive surface charge layer, as shown in Fig. 7c, and the
554 microscopic high electric field on the rock surface may have caused air molecules to be ionized.
555 The field ionization of air molecules ($O_2 \rightarrow O_2^+ + e^-$) produced O_2^+ ions and electrons. At stage
556 IV, the applied stress on the lower part might be concentrated locally because the structure of this
557 sub-volume was changed by the multiple global fractures. Consequently, part of the sub-volume
558 became less stressed or unstressed (Fig. S6), and the positive holes were transmitted to the surface.
559 Therefore, as illustrated in Fig. 7c, the battery polarity was reversed; the upper part became the
560 cathode due to the ionization electrons, and the lower part became the anode due to the
561 accumulation of positive holes, leading to the negative fluctuation of the detected PSRC.
562 Meanwhile, the physical processes of several positive or negative fluctuations in certain specimens
563 are difficult to illustrate clearly because the structures, deformations, and stress concentrations at
564 such a short stage are complex and often transient. Basically, the significant and abnormal

565 variations of PSRC were contributed comprehensively by the physical processes mentioned and
566 discussed above.

567 **5 Conclusions**

568 By uniaxially compressing cubic- and conical-shaped diorite specimens to failure and pasting
569 copper foil on large parts of the rock surface for the first time, this study synchronously measured
570 the pressure-stimulated rock current (PSRC) and acoustic emission (AE). The experimental results
571 revealed that the temporal variation of the PSRC of the diorite specimen could be divided into
572 three phases: (1) indistinctive at stages of elastic deformation and early micro-fracturing, (2) step-
573 like rise at a high level of stress and significant accumulated damage, and (3) dramatic oscillation
574 shortly prior to impending rock failure.

575 The stress-activated P-hole activation, crack charge separation, and field emission of electrons
576 are suggested responsible for the PSRC variations, and the prominent mechanism might be
577 different in varied phases of the PSRC evolution. The coalescence of local microcracks and its
578 connection to global fractures provided important channels for the movement of electric charges
579 and consequently promoted remarkable PSRC variations. The experimental results of this study
580 provide a new understanding of the stress-activated electric current of compressively loaded rocks
581 embodied with peroxy minerals, which exhibit potential use of dynamic signal detection of PSRC
582 and possible precursor identification of rock fracturing, which includes but not limited to rock
583 mass breaking, rock structure failure, mine burst, and seismic activity.

584 **Acknowledgments**

585 This research was supported by the Key Program of National Nature Science Foundation of China
586 (41930108), National Nature Science Foundation of China (42101394), Project funded by China
587 Postdoctoral Science Foundation (2021M693550)

588 **References**

- 589 1. Anastasiadis, C. , Triantis, D. , Hogarth, C. A. (2007). Comments on the phenomena underlying pressure
590 stimulated currents in dielectric rock materials. *Journal of Materials Science*, 42(8), 2538-2542.
- 591 2. Atkinson, B. K. (1987). *Fracture mechanics of rock*. Amsterdam, The Kingdom of the Netherlands: Elsevier.
- 592 3. Balk, M. , Bose, M. , Ertem, G. , Rogoff, D. A. , Rothschild, L. J. , & Freund, F. T. (2009). Oxidation of
593 water to hydrogen peroxide at the rock–water interface due to stress-activated electric currents in rocks.
594 *Earth and Planetary Science Letters*, 283(1-4), 87-92. <https://doi.org/10.1016/j.epsl.2009.03.044>
- 595 4. Dickinson, J. T. , Donaldson, E. E. , & Park, M. K. (1981). The emission of electrons and positive ions from
596 fracture of materials. *Journal of Materials Science*, 16, 2897-2908. <https://doi.org/10.1007/BF00552976>
- 597 5. Enomoto, Y. , & Hashimoto, H. (1990). Emission of charged particles from indentation fracture of rocks.
598 *Nature*, 346, 641-643. <https://doi.org/10.1038/346641a0>
- 599 6. Enomoto, Y. , & Hashimoto, H. (1992). Transient electrical activity accompanying rock under indentation
600 loading. *Tectonophysics*, 211, 337-344. [https://doi.org/10.1016/0040-1951\(92\)90069-1](https://doi.org/10.1016/0040-1951(92)90069-1)
- 601 7. Fonseka, G., Murrell, S. , & Barnes, P. (1985). Scanning electron microscope and acoustic emission studies
602 of crack development in rocks. *International Journal of Rock Mechanics and Mining Sciences &*
603 *Geomechanics Abstracts*, 55, 273-289. [https://doi.org/10.1016/0148-9062\(85\)92060-1](https://doi.org/10.1016/0148-9062(85)92060-1)
- 604 8. Freund, F. T. (2002). Charge generation and propagation in igneous rocks. *Journal of Geodynamics*, 33(4-5),
605 543-570. [https://doi.org/10.1016/S0264-3707\(02\)00015-7](https://doi.org/10.1016/S0264-3707(02)00015-7)

- 606 9. Freund, F. T. (2009). Stress-activated positive hole charge carriers in rocks and the generation of pre-
607 earthquake signal. *Electromagnetic phenomena associated with earthquakes*, 41-96.
- 608 10. Freund, F. T. , Takeuchi, A. , Lau, B. W. (2006). Electric currents streaming out of stressed igneous rocks–
609 A step towards understanding pre-earthquake low frequency EM emissions. *Physical and Chemistry of the*
610 *Earth, Parts A/B/C*, 31, 4-9. <https://doi.org/10.1016/j.pce.2006.02.027>
- 611 11. Gallagher Jr, J. J. , Friedman, M. , Handin, J. , & Sowers, G. M. (1974). Experimental studies relating to
612 microfracture in sandstone. *Tectonophysics*, 21(3), 203-247. [https://doi.org/10.1016/0040-1951\(74\)90053-5](https://doi.org/10.1016/0040-1951(74)90053-5)
- 613 12. Hadjicontis, V. , & Mavromatou, C. (1994). Transient electric signals prior to rock failure under uniaxial
614 compression. *Geophysical Research Letters*, 21(16), 1687-1690. <https://doi.org/10.1029/94GL00694>
- 615 13. Hoenig, S. A. (1979). Aerosol anomalies preceding earthquakes. *Nature*, 279, 169-169.
616 <https://doi.org/10.1038/276606a0>
- 617 14. Kurita, K. , & Fujii, N. (2013). Stress memory of crystalline rocks in acoustic emission. *Geophysical*
618 *Research Letters*, 6(1), 9-12. <https://doi.org/10.1029/GL006i001p00009>
- 619 15. Li, D. X. , Wang, E. Y. , Ju, Y. Q. , & Wang, D. M. (2021a). Laboratory investigations of a new method
620 using pressure stimulated currents to monitor concentrated stress variations in coal. *Natural Resources*
621 *Research*, 30, 707-724. <https://doi.org/10.1007/s11053-020-09749-6>
- 622 16. Li, D. X. , Wang, E. Y. , Li, Z. H. , Ju, Y. Q. , Wang, D. M., & Wang, X. Y. (2021b). Experimental
623 investigations of pressure stimulated currents from stressed sandstone used as precursors to rock fracture.
624 *International Journal of Rock Mechanics and Mining Sciences*, 145.
625 <https://doi.org/10.1016/j.ijrmms.2021.104841>
- 626 17. Li, M. , Wang, H. T. , Wang, D. M. , Shao, Z. L. (2020). Experimental study on characteristics of surface
627 potential and current induced by stress on coal mine sandstone roof. *Engineering Geology*, 266.
628 <https://doi.org/10.1016/j.enggeo.2019.105468>
- 629 18. Li, Z. , Wang, E. , & He, M. (2015). Laboratory studies of electric current generated during fracture of coal
630 and rock in rock burst coal mine. *Journal of Mining*, 2015. <http://dx.doi.org/10.1155/2015/235636>
- 631 19. Liao, C. T. , Zhang, C. S. , Wu, M. L. , Ma, Y. S. , & Ou, M. Y. (2003). Stress change near the Kunlun fault
632 before and after the Ms 8.1 Kunlun earthquake. *Geophysical research letters*, 30(20).
633 <https://doi.org/10.1029/2003GL018106>
- 634 20. Meng, W. , Chen, Q. C. , Zhao, Z. , Wu, M. L. , Qin, X. H. , & Zhang, C. Y. (2015). Characteristics and
635 implications of the stress state in the Longmen Shan fault zone, eastern margin of the Tibetan plateau.
636 *Tectonophysics*, 656, 1-19. <https://doi.org/10.1016/j.tecto.2015.04.010>
- 637 21. Mizutani, H. , Ishido, T. , Yokokura, T. , & Ohnishi, S. (1976). Electrokinetic phenomena associated with
638 earthquakes. *Geophysical Research Letters*, 3(7), 365-368. <https://doi.org/10.1029/GL003i007p00365>
- 639 22. Olsson, W. A. , & Peng, S. S. (1976). Microcrack nucleation in marble. *International Journal of Rock*
640 *Mechanics and Mining Sciences & Geomechanics Abstracts*, 13, 53-59. [https://doi.org/10.1016/0148-9062\(76\)90704-X](https://doi.org/10.1016/0148-9062(76)90704-X)
- 641
- 642 23. Pasiou, E. D. , & Triantis, D. (2017). Correlation between the electric and acoustic signals emitted during
643 compression of brittle materials. *Frattura ed Integrità Strutturale*, 11, 41-51. <https://doi.org/10.3221/IGF-ESIS.40.04>
- 644
- 645 24. Rossman, G. R. (1996). Studies of OH in nominally anhydrous minerals. *Physics and Chemistry of Minerals*,
646 23, 299-304. <https://doi.org/10.1007/BF00207777>
- 647 25. Saltas, V. , Vallianatos, F. , Triantis, D. , Stavrakas, I. (2018). Complexity in laboratory seismology: From
648 electrical and acoustic emissions to fracture. *Complexity of seismic time series*(pp. 239-273). Amsterdam,
649 The Kingdom of the Netherlands: Elsevier.
- 650 26. Scholz, C. H. (1968). Microfracturing and the inelastic deformation of rock in compression. *Journal of*
651 *Geophysical Research*, 73(4), 1417-1432. <https://doi.org/10.1029/JB073i004p01417>

- 652 27. Scoville, J. , Sornette, J. , & Freund, F. T. (2015). Paradox of peroxy defects and positive holes in rocks Part
653 II: Outflow of electric currents from stressed rocks. *Journal of Asian Earth Sciences*, 114, 338-351.
654 <https://doi.org/10.1016/j.jseaes.2015.04.016>
- 655 28. Simons, G. , & Richter, D. (1976). *The physics and chemistry of minerals and rocks*. State of New Jersey,
656 the United States of America: Wiley-Interscience.
- 657 29. Slifkin, L. (1993). Seismic electric signals from displacement of charged dislocations. *Tectonophysics*,
658 224(1-3), 149-152. [https://doi.org/10.1016/0040-1951\(93\)90066-S](https://doi.org/10.1016/0040-1951(93)90066-S)
- 659 30. Sprunt, E. S. , & Brace, W. F. (1974). Direct observation of microcavities in crystalline rocks. *International*
660 *Journal of Rock Mechanics and Mining Sciences & Geomechanics Abstracts*, 11, 139-150.
661 [https://doi.org/10.1016/0148-9062\(74\)92874-5](https://doi.org/10.1016/0148-9062(74)92874-5)
- 662 31. Stavrakas, I. , Triantis, D. , Agioutantis, Z. , Maurigiannakis, S. , Saltas, V. , Vallianatos, F. , & Clarke, M.
663 (2004). Pressure stimulated currents in rocks and their correlation with mechanical properties. *Natural*
664 *Hazards and Earth System*, 4, 563-567. <https://doi.org/10.5194/nhess-4-563-2004>
- 665 32. Stergiopoulos, C. , Stavrakas, I. , Hloupis, G. , Triantis, D. , & Vallianatos, F. (2013). Electrical and acoustic
666 emissions in cement mortar beams subjected to mechanical loading up to fracture. *Engineering Failure*
667 *Analysis*, 35, 454-461. <https://doi.org/10.1016/j.engfailanal.2013.04.015>
- 668 33. Tapponnier, P. , & Brace, W. F. (1976). Development of stress-induced microcracks in Westerly granite.
669 *International Journal of Rock Mechanics and Mining Sciences & Geomechanics Abstracts*, 13, 103-112.
670 [https://doi.org/10.1016/0148-9062\(76\)91937-9](https://doi.org/10.1016/0148-9062(76)91937-9)
- 671 34. Triantis, D. , Stavrakas, I. , Anastasiadis, C. , Kyriazopoulos, A. , & Vallianatos, F. (2006). An analysis of
672 pressure stimulated currents (psc), in marble samples under mechanical stress. *Physical and Chemistry of the*
673 *Earth, Parts A/B/C*, 31, 4-9. <https://doi.org/10.1016/j.pce.2006.02.018>
- 674 35. Triantis, D. , Stavrakas, I. , Kyriazopoulos, A. , Hloupis, G. , & Agioutantis, Z. (2012). Pressure stimulated
675 electrical emissions from cement mortar used as failure predictors. *International Journal of Fracture*, 175,
676 53-61. <https://doi.org/10.1007/s10704-012-9701-7>
- 677 36. Uyeda, S. , Hayakawa, M. , & Nagao, T. (2002). Electric and magnetic phenomena observed before the
678 volcano-seismic activity in 2000 in the Izu island region, Japan. *Proceedings of the national academy of*
679 *seiences of the United States of America*, 99 (11), 7352-7355. <https://doi.org/10.1073/pnas.072208499>
- 680 37. Vallianatos, F. , & Tzanis, A. (1998). Electric current generation associated with the deformation rate of a
681 solid: preseismic and coseismic signals. *Physical and Chemistry of the Earth*, 23(9-10), 933-938.
682 [https://doi.org/10.1016/S0079-1946\(98\)00122-0](https://doi.org/10.1016/S0079-1946(98)00122-0)
- 683 38. Vallianatos, F. , Triantis, D. , Tzanis, A. , Anastasiadis, C. , & Stavrakas, L. (2004). *Physics and Chemistry*
684 *of the Earth, Parts A/B/C*, 29(4-9), 339-351. <https://doi.org/10.1016/j.pce.2003.12.003>
- 685 39. Viktorov, S. , & Kochanov, N. (2016). Experimental regularities in formation of submicron particles under
686 rock failure. *Journal of Mining Science*, 52, 899-905. <https://doi.org/10.1134/S1062739116041370>
- 687 40. Wang, H. F. , & Heard, H. C. (1985). Prediction of elastic moduli via crack density in pressurized and
688 thermally stressed rock. *Journal of Geophysical Research: Solid Earth*, 90(B12), 10342-10350.
689 <https://doi.org/10.1029/JB090iB12p10342>
- 690 41. Warwick, J. W. , Stoker, C. , & Meyer, T. R. (1982). Radio emission associated with rock fracture: possible
691 application to the great Chilean earthquake of May 22, 1960. *Journal of Geophysical Research: Solid Earth*,
692 87(B4), 2851-2859. <https://doi.org/10.1029/JB087iB04p02851>
- 693 42. Whitworth, R. W. (1975). Charged dislocations in ionic crystals. *Advances in Physics*, 24, 203-204.
694 <https://doi.org/10.1080/00018737500101401>
- 695 43. Yoshida, S. , Clint, O. C. , & Sammonds, P. R. (1998). Electric potential changes prior to shear fracture in
696 dry and saturated rocks. *Geophysical Research Letters*, 25(10), 1577-1580. <https://doi.org/10.1029/98GL01222>
697

- 698 44. Yoshida, S. , Uyeshima, M. , & Nakatani, M. (1997). Electric potential changes associated with slip failure
699 of granite: preseismic and coseismic signals. *Journal of Geophysical Research: Solid Earth*, 1021(B7),
700 14883-14897. <https://doi.org/10.1029/97JB00729> .